HHS Public Access

Author manuscript

NanoImpact. Author manuscript; available in PMC 2019 September 20.

Published in final edited form as:

NanoImpact. 2018 January ; 9: 72–84. doi:10.1016/j.impact.2017.10.006.

Carbon nanotubes physicochemical properties influence the overall cellular behavior and fate

Reem Eldawud[a], **Alixandra Wagner**[a], **Chenbo Dong**[a], **Todd A. Stueckle**[b], **Yon Rojanasakul**[c], **Cerasela Zoica Dinu**[a,c,*]

[a]Department of Chemical and Biomedical Engineering, West Virginia University, Morgantown, WV 26506, USA

[b]Health Effects Laboratory Division, National Institute for Occupational Safety and Health, Morgantown, WV 26505, USA

[c]Department of Pharmaceutical Sciences, West Virginia University, WV 26506, USA

Abstract

The unique properties of single walled carbon nanotubes (SWCNTs) make them viable candidates for versatile implementation in the next generation of biomedical devices for targeted delivery of chemotherapeutic agents or cellular-sensing probes. Such implementation requires user-tailored changes in SWCNT's physicochemical characteristics to allow for efficient cellular integration while maintaining nanotubes' functionality. However, isolated reports showed that user-tailoring could induce deleterious effects in exposed cells, from decrease in cellular proliferation, to changes in cellular adhesion, generation of reactive oxygen species or phenotypical variations, just to name a few. Before full implementation of SWCNTs is achieved, their toxicological profiles need to be mechanistically correlated with their physicochemical properties to determine how the induced cellular fate is related to the exposure conditions or samples' characteristics. Our study provides a comprehensive analysis of the synergistic cyto- and genotoxic effects resulted from short-term exposure of human lung epithelial cells to pristine (as manufactured) and user-tailored SWCNTs, as a function of their physicochemical properties. Specifically, through a systematic approach we are correlating the nanotube uptake and nanotube-induced cellular changes to the sample's physicochemical characteristics (e.g., metal impurities, length, agglomerate size, surface area, dispersion, and surface functionalization). By identifying changes in active hallmarks involved in cell-cell connections and maintaining epithelial layer integrity, we also determine the role that short-term exposure to SWCNTs plays in the overall cellular fate and cellular transformation. Lastly, we assess cellular structure-function relationships to identify non-apoptotic pathways induced by SWCNTs exposure that could however lead to changes in cellular behavior and cellular transformation. Our results show that the degree of cell transformation is a function of

* Corresponding author at: Department of Chemical and Biomedical Engineering, West Virginia University, Benjamin M. Statler College of Engineering and Mineral Resources, PO Box 6102, Morgantown, WV, 26506, USA. cerasela-zoica.dinu@mail.wvu.edu (C.Z. Dinu).

Disclaimer

Research findings and conclusions are those of the authors and do not necessarily represent the views of the National Institute for Occupational Safety and Health. The authors declare no competing financial interest.

Appendix A. Supplementary data

Supplementary data to this article can be found online at https://doi.org/10.1016/j.impact.2017.10.006.

the physicochemical properties of the SWCNT, with the nanotube with higher length, higher metal content and larger agglomerate size reducing cell viability to a larger extent. Such changes in cell viability are also complemented by changes in cell structure, cycle and cell-cell interactions, all responsible for maintaining cell fate.

Keywords

Single walled carbon nanotubes (SWCNTs); User-tailoring; Human lung epithelial cells; Physicochemical properties; Synergistic effects

1. Introduction

Engineered carbon-based nanomaterials such as fullerenes, nanodiamonds, carbon nanofibers and nanotubes (CNTs) exhibit unique physical, chemical, optical and electrical properties (Mauter and Elimelech, 2008; Jorio and Dresselhaus, 2003) that make them attractive candidates for a variety of applications. In particular, single walled carbon nanotube (SWCNTs) have been proposed for the development of the next generation of bio-based platforms for healthcare applications (Mehdipoor et al., 2011; Wu et al., 2010; Wen et al., 2015), for controlled and targeted delivery of chemotherapeutic agents (Liu et al., 2007), antimicrobials (Benincasa et al., 2011), and antibodies (Podesta et al., 2009), or for biosensing probe development respectively (Wen et al., 2015). However, in order to meet the demands of such specific biomedical applications (Dong et al., 2013; Dong et al., 2014a), SWCNTs physicochemical properties need to be readily and specifically user-tailored. For instance, the application of SWCNTs as drug delivery nanovehicles requires the ability to effectively load and unload molecular agents (therapeutic molecules or targeting moieties) onto the nanotubes while maintaining their functionality and stability at the nanovehicle interface itself, (Karimi et al., 2015) as well as increased cellular integration upon uptake (Dong et al., 2014a; Dong et al., 2015).

To tailor the properties of SWCNTs, several chemical strategies have been developed; specifically, using both gas and liquid-phase activation (Guo et al., 2010), or oxidation with strong oxidants such nitric and/or sulfuric acid (Dong et al., 2013), or hydrogen peroxide (Zehua and Guojian, 2012), the creation of surface functional groups including carboxyl (COOH) (Eldawud et al., 2015a; Zehua and Guojian, 2012), carbonyl (CO) (Li and Li, 2011), and phenol (Georgakilas et al., 2008) was demonstrated. Among such modification techniques, nitric and sulfuric acids treatment is regarded as the most common and prevalent functionalization method due to its feasibility, convenience, and reproducibility (Wepasnick et al., 2011). Such acids treatment is known to generate SWCNTs that are shorter, more hydrophilic, of higher purity, and with lower tendency to agglomerate in aqueous solutions. The acids treatment strategy is also known to facilitate higher loadings and functionality retention of selected immobilized proteins such as soybean peroxidase (SBP) or bovine serum albumin (BSA) which allowed for the SWCNTs vehicles possible implementation in applications similar to the ones previously listed (Dong et al., 2013; Dong et al., 2014a; Campbell et al., 2014).

However, analyses revealed that upon acids treatment, the SWCNT's physicochemical properties change and resulting O-derived surface functionalization for instance could induce major deleterious effects upon nanotubes interaction with cellular systems (Dong et al., 2013; Dong et al., 2014a; Eldawud et al., 2015a; Manke et al., 2014). Specifically, O-functionalized SWCNTs, while exhibiting a higher solubility relative to their pristine (non-functionalized) counterparts, are known to generate active oxidation centers that result in increased ion-exchange, piezoelectric charge and non-specific adsorption of biomolecules (Atieh et al., 2010). Furthermore, studies have showed that exposure to functionalized SWCNTs leads to high micronuclei frequency (Visalli et al., 2015; Sargent et al., 2010), a decrease in cellular proliferation (Dong et al., 2014b), and significant effects on cellular adhesion (Eldawud et al., 2015a), however with minimum negative consequences on cellular viability (Hitoshi et al., 2011). In contrast, cellular exposure to pristine SWCNTs led to a significant reduction in the viability of immortalized and primary human lung epithelial cells (Herzog et al., 2009; Siegrist et al., 2014), and generation of reactive oxygen species and lipid hydroperoxides (Dong et al., 2015; Visalli et al., 2015). Such effects are known to influence the cellular fate and possibly lead to cellular transformation. Such transformation could potentially be translated into loss in cell-cell contacts and the epithelial layer integrity, with the loss in cellular connections and adhesion properties in anchored-dependent cells being known to guide activation of various molecular pathways and malignant phenotypic changes, as well as lead to gains in mesenchymal properties, apoptosis and premature senescence respectively (Adhikary et al., 2014; Smit and Peeper, 2010). For example, epithelial-to-mesenchymal transition (EMT) was previously shown to be characterized by down regulation of epithelial cadherin and Rho family small proteins (i.e., E-cadherin and Rac), as well as the acquisition of migratory and motile properties of cells (Adhikary et al., 2014; Smit and Peeper, 2010; Lovisa et al., 2015). Furthermore, previous studies have showed that changes in the epithelial integrity and loss in cell-cell contacts could be leading to changes in the cellular behavior (Jean and Simmons, 1999) to be potentially associated with carcinogenesis (Knights et al., 2012; Kalluri and Weinberg, 2009) upon nanotubes' complex interactions with cytoskeletal elements microtubules or actin (Pawlak and Helfman, 2001). Complementary, cellular apoptosis was identified as a failsafe mechanism known to require phenotypic changes mostly involving cell cycle arrest at the G1 phase. (Plati et al., 2011). However, these reports accounted mainly the effects upon cellular exposure to isolated SWCNTs and such limited mechanistic correlations were made between how user-tailoring of their surfaces for instance affects or changes toxicological profiles of the functionalized sample relative to pristine one. If it is to establish a reliable platform that allow for integrative implementation of SWCNTs in biomedical applications, a systematic assessment of the structure-function relationships related to both cellular activity and cellular transformation as a function of the ability to tailor SWCNTs' physicochemical properties needs to be developed.

Herein we hypothesized that human lung epithelial cells exposed to nanotubes with user-tailored physicochemical properties, such as surface chemistry and length, are undergoing cellular transformations via non-apoptotic pathways (Plati et al., 2011). To test this hypothesis, we investigated how short-term exposure to a user-created library of SWCNTs affects the expression of regulatory proteins playing key roles in establishing cellular

connections, maintaining epithelial layer integrity, known as active hallmarks for EMT and related to cell transformation and cancer progression. Through a multi-parametric approach we differentiate the influence of such physicochemical properties on overall cellular fate and identify the conditions that determine toxicity both through independent and synergistic pathways. Our results demonstrate that changes in the SWCNTs' physicochemical properties changes cell viability, alter cell cycle, as well as cell-cell connections and migration pathways in the exposed cells. Further, our results hint that consideration needs to be given when user-controlled strategies are employed for nanotube functionalization so that their deleterious effects are circumvented.

2. Materials and methods

2.1. Single walled carbon nanotubes (SWCNTs) acid treatment

User-tailored SWCNTs were obtained by liquid phase oxidation of commercial, i.e., pristine SWCNTs (Unidym Inc.). Specifically, pristine SWCNTs were incubated in a mixture of 3:1 (*v*/v) concentrated sulfuric (Fisher Scientific, 96.4%) and nitric acid (Fisher Scientific, 69.6%) for different periods determined by the user (i.e., 3 and 6 h) to obtain SWCNTs with different degrees of O-related functionalities and lengths (from here on, such nanotubes will be referred to as user-tailored SWCNTs) (Campbell et al., 2013). Upon time elapsed, the SWCNTs/acid mixture was diluted in deionized water and filtered through a GTTP filter membrane, (0.2 μm pore size, Fisher Scientific). The nanotubes on the filter were subsequently washed extensively with deionized water, dried under vacuum and stored until further use.

2.2. Materials characterization

Raman spectroscopy was used to investigate the physicochemical properties of the user-tailored samples. For this, SWCNT dry samples (pristine, 3 and 6 h treated samples) were deposited onto clean glass slides and scanned using a Raman spectrometer (CL532–100, 100 mW, USA) and a 532 nm green laser with a spot size of $< 0.01\ mm^2$ directed though a 50× objective. Detailed scans were taken in the 100 to 3200 cm^{-1} range and low energy laser (i.e., < 0.5 mV); short exposure times (10 s) were maintained to prevent unexpected heating effects of the samples.

Atomic force microscopy (AFM) and air tapping mode was used to investigate the lengths of the SWCNTs samples (Marshall et al., 2006). Briefly, commercial Si tips (Asylum Research, AC240TS) were employed at a resonance frequency varying from 50 to 90 kHz. During the scanning process, the topography, phase and amplitude images of the samples were collected simultaneously. A minimum of 3 scans were obtained for each sample being analyzed and at least 30 individual nanotubes were measured to obtain an average of their length distribution.

Energy dispersive X-ray spectroscopy (EDX) was employed for quantitative elemental analysis of the SWCNT samples. For this, dry samples were mounted onto silica wafers and their elemental composition was evaluated using a Hitachi S-4700 field emission scanning

electron microscope with a S-4700 detector integrating secondary (SE) and backscattered (BSE) electron detection (in a single unit).

Analyses of SWCNT-induced agglomerate sizes were performed using a dynamic light scattering device (DLS, DelsaTM). For this, suspensions of 50 μg/ml samples (pristine, 3 and 6 h treated SWCNTs respectively) were prepared in Dulbecco Minimum Essential Media (DMEM) supplemented with 5% fetal bovine serum (FBS), and scanned at 20 °C. For each sample, 150 measurements were recorded and the mean sample diameter was calculated by evaluating the intensity, volume, and number distribution data being collected.

The dispersity of samples in both distilled water and DMEM supplemented with 5% FBS was investigated using standard protocols (Dong et al., 2013). Briefly, samples were prepared in the corresponding solvent to yield to 3 mg/ml suspensions that was further sonicated for 2 min and centrifuged for 5 min at 3000 rpm. Subsequently, 0.8 ml supernatant was removed and filtered through a 0.2 μm GTTP filter membrane. The membrane was then dried under vacuum and the weight of the isolated nanotubes was evaluated. The solubility of the samples in different solvents was calculated based on the initial starting weight and final weight of the filter paper, as well as volume used for suspension.

2.3. Immobilization of fluorescent proteins onto SWCNTs

Alexa Fluor 488 bovine serum albumin (Alexa-BSA, Sigma) was used to fluorescently label the nanotubes (Dong et al., 2013; Campbell et al., 2013) either through physical (for pristine SWCNTs) or covalent (for 3 and 6 h acids treated SWCNTs) chemistry respectively. Briefly, pristine SWCNTs were dispersed and incubated in 1 mg/ml Alexa-BSA solution in phosphate buffered saline (PBS, Lonza) for 2 h at room temperature and 200 rpm (Kah et al., 2014), while the treated SWCNTs were first dispersed by sonication for 2 min in 160 mM 1-ethyl-3-[3-dimethylaminopropyl] carbodiimide hydrochloride (EDC, Acros Organics) and 80 mM N-hydroxysuccinimide (NHS, Pierce) suspended in 2-(N-morpholino) ethanesulfonic acid sodium salt buffer (MES, 50 mM, pH 4.7, Sigma) for 15 min, at room temperature and 200 rpm (Dong et al., 2015). Subsequently, the EDC/NHS activated SWCNTs were filtered through a 0.2 μm GTTP membrane, washed thoroughly with MES buffer, re-suspended in 1 mg/ml Alexa-BSA by brief sonication, and incubated for 3 h at room temperature and 200 rpm. The resulting Alexa-BSA-SWCNT conjugates (either from the physical or covalent binding) were again filtered and washed with excessive amounts of PBS to remove any unbound proteins. The supernatant and first 2 washes were collected and used to quantify protein loading. To avoid dye photobleaching, all samples were kept away from light at all times.

2.4. Protein loading and functionality analysis

The amount of Alexa-BSA loaded onto the SWCNTs (either pristine or treated samples) was evaluated using standard bicinchoninic acid assay (BCA, Pierce). Specifically, 50 μl of the collected supernatant or individual washes were incubated with 1 ml of working reagent prepared by mixing 50 parts of reagent A (BCA protein assay reagent A formed with bicinchonic acid and tartrate in an alkaline carbonate buffer) with 1 part of reagent B (BCA protein assay reagent B formed with 4% copper sulfate pentahydrate solution) for 30 min at

37 °C. The absorbance values for all samples were read using a spectrophotometer (Evolution 300/600, Thermo Fisher) at 562 nm wavelength. Control calibration curves were performed using serial dilutions of free Alexa-BSA in the working buffer. The relative amount of Alexa-BSA immobilized onto SWCNTs or the loaded protein was estimated by calculating the difference between the amount of protein initially offered to the sample during the incubation step and the amount of the protein removed in the supernatant and 2 subsequent washes respectively.

The functionality of Alexa-BSA immobilized onto the samples was evaluated by measuring the emission efficiency of the fluorophore of the immobilized protein relative to the one of the free protein in solution (Campbell et al., 2014; Smith et al., 2014). Briefly, the absorbance spectra of 100 μg/ml of Alexa-BSA-SWCNT conjugates prepared in PBS was evaluated relative to both the absorbance spectra of unlabeled SWCNTs as well as the one of free Alexa-BSA. The absorbance spectrum of immobilized Alexa-BSA (excitation at 488 nm and emission at 515 nm) was calculated from the difference between the absorbance values of the Alexa-BSA-SWCNTs and that of the unlabeled SWCNTs. The functionality of the immobilized Alexa-BSA was determined by measuring the height of the absorbance peaks relative to the height of the peaks of free Alexa-BSA in solution.

2.5. Cell culture and cellular exposure to SWCNTs

Immortalized human lung epithelial cells (BEAS-2B, American Type Culture Collection-ATCC) were cultured in DMEM supplemented with 5% FBS, 2 mM L-glutamine and 100 units/ml penicillin/streptomycin (Invitrogen). Cells were passaged regularly and kept in 5% CO_2 at 37 °C.

For cellular exposure, pristine and user-tailored SWCNTs were first suspended in deionized water by sonication until all large agglomerates were completely dispersed (visual assessment). Subsequently, the samples were filtered, resuspended in DMEM media with 5% FBS, and sonicated for 2 min to form stable dispersions. Based on the recommendation made by the Occupational Safety and Health Administration (OSHA) for particles less than 5 μm in diameter, an exposure dose of 50 μg/ml sample was chosen for assessment. The dose reflects acute worker exposures for 14 years at 40 working hour a week and is similar both to the levels of SWCNTs currently recorded in working areas (ranging between 0.7 and 53 $\mu g/m^3$) as well as to estimates of SWCNTs on individual worker gloves (ranging between 217 μg to 6020 μg) (Maynard et al., 2004a; Jeong Hee et al., 2008a).

2.6. Evaluation of the SWCNTs cellular uptake

BEAS-2B cells were seeded overnight in a 12-well plate (Fisher) at 2.5×10^5 cell/well and exposed to 50 μg/ml Alexa-BSA-SWCNT conjugates dispersed in cellular media by brief sonication (intervals of 10 s were used to avoid loss of protein functionality (Stepanskiy, 2012) or reduction of the fluorophore intensity) (Welsher et al., 2009). Controls (i.e., unexposed cells, cells exposed to unlabeled SWCNTs, and cells exposed to free Alexa-BSA at equivalent amounts to the amount of protein loaded onto the samples) were performed in parallel. After 24 h incubation, the exposed cells were washed with PBS, collected, and centrifuged at 1200 rpm for 5 min to remove any free proteins, noninternalized or loosely

bound SWCNTs or SWCNT-based conjugates (the procedure was repeated twice). Subsequently, the exposed cells were washed again with PBS, fixed with 4% glutaraldehyde solution (Fisher Scientific) for 15 min at room temperature, and then again extensively washed with PBS to remove excess glutaraldehyde solution.

Fluorescence-activated cell sorting (FACS) of the exposed cells was performed on a BD FACS Caliber flow cytometer (Becton Dickinson). FITC signal used excitation at 488 nm and emission at 515 nm and 10,000 events were recorded for each sample. Data was analyzed and plotted using FlowJo v7.2.5 software.

2.7. Cell viability analysis

Percentage of apoptotic and necrotic cells was analyzed using established protocols based on TACS Annexin V-FITC apoptosis detection kit (R&D Systems). Specifically, BEAS-2B cells were seeded overnight onto a 12-well plate at 2.5×10^5 cell/well and exposed to 50 μg/ml pristine or treated SWCNTs for 24 h. Subsequently, the exposed cells were washed with PBS, harvested, centrifuged at 1200 rpm for 5 min, and stained with 5 μl Annexin V-FITC and 1 μl propidium iodide (PI) prepared in ice-cold 1 × binding buffer for 15 min (all reagents found in the kit). Next, the exposed cells were washed again and analyzed using FACS excitation of 488 nm and emission wavelengths of 530 nm for FITC fluorescence, and 610 nm for PI fluorescence respectively. At least 10,000 events were again recorded for each cell sample being analyzed. The percentages of viable (PI−, Annexin−), apoptotic (PI−, Annexin+) and necrotic cells (PI+, Annexin+) were evaluated using FlowJo v7.2.5 software. Since double labeling was performed, compensation was set using cells stained solely with PI or the FITC-conjugated Annexin V respectively.

2.8. Cell membrane imaging

BEAS-2B cells were seeded overnight on glass coverslips in a 12 well plate at 1.5×10^5 cell/well and exposed to 50 μg/ml pristine or treated SWCNTs for 24 h. Subsequently, the exposed cells were washed twice with Hank's balanced salt solution (HBSS, Corning), and fixed with 4% formaldehyde (Sigma-Aldrich) for 15 min at 37 °C. Upon fixation, the exposed cells were washed again 3 times with HBSS and stained with 3 μg/ml Alexa Fluor 594 wheat germ agglutinin (WGA) and 2 μM Hoechst 33,342 (Image-iT LIVE plasma membrane and nuclear labeling kit, Life Technologies) respectively for 10 min. Lastly, the coverslips with stained cells were washed twice with HBSS, mounted on glass slides, and imaged using a fluorescence microscope (Leica) and a 40 × objective.

2.9. Cell nuclear deformation

BEAS-2B cells were seeded overnight onto a 12-well plate at a density of 2.5×10^5 cell/well and exposed to cellular media containing suspensions of 50 μg/ml pristine or treated SWCNTs for 24 h. Subsequently, the exposed cells were incubated with 10 μg/ml of Hoechst 33,342 (Molecular Probes) for 30 min at 37 °C, washed twice with PBS, and analyzed using fluorescence microscopy (Leica) to assess the percentage of cells showing deformation in nuclear morphology, intensely condensed chromatin, and/or fragmented nuclei.

2.10. Western blot analysis

BEAS-2B cells were seeded in a 6-well plate (Fisher) at 5×10^6 cell/well and exposed to suspensions of 50 μg/ml samples (either pristine or treated SWCNTs) in cellular media for 24 h. Following exposure, the cells were lysed for 30 min in lysis buffer containing 2% triton X-100, 1% sodium dodecyl sulfate (SDS), 100 mM sodium chloride (NaCl), 10 mM *tris*-hydrochloric acid (HCl), completed with mini cocktail pro-tease inhibitors (all reagents were purchased from Roche) and 1 mM ethylenediamine tetraacetic acid (EDTA, Molecular Probes). The supernatant was collected and the protein content was determined using the BCA assay as described previously (Eldawud et al., 2014). Complementarily, the supernatant was separated by a 10% SDS-PAGE gel and transferred to polyvinylidene fluoride (PVDF) membranes using the iBlot® dry blotting system (Invitrogen). Membranes were blocked in 5% skim milk in *tris*-buffered saline (TBST, 25 mM *Tris*–HCl, 125 mM NaCl, and 0.1% Tween-20; Sigma Chemicals) for 1 h at room temperature, and subsequently incubated with primary antibody (Cdc 2, Cdc 25a, E-cadherin, Rac 1/2/3, vimentin or vinculin, all purchased from Cell Signaling) at 4 °C overnight, washed 3 times with PBS containing 1% Tween-20 with 10 min for each wash, and then again incubated with horseradish peroxidase-conjugated secondary antibody (Cell Signaling) for 1 h and at room temperature.

Finally, the samples were analyzed by chemiluminescence (Supersignal) and band quantification was performed via densitometry analysis and using ImageJ software, version 10.2.

2.11. Cell migration assay

BEAS-2B cells were seeded overnight in a 12-well plate at 2.5×10^5 cell/well and exposed to 50 μg/ml pristine or treated SWCNTs for 24 h. Porous membranes (8 μm pore size; Becton Dickinson) were hydrated in cell culture media for 2 h at 37 °C and 5% CO_2 atmosphere. In preparation for the transfer onto membranes, cells were suspended in a serum free media, counted to 2×10^4 live cells and seeded onto such porous membranes for 24 h. During that time, the inserts containing the membranes were immersed in a 24 well plates containing 5% FBS media. Upon time elapsed, migrated cells were stained and fixed using Diff-Quick stain kit (Invitrogen); this was achieved by sequentially transferring the membrane inserts through 3 solutions provided with the kit, followed by 2 water rinses in between. The cell culture inserts were subsequently allowed to air dry upside down, overnight and at room temperature. Images were obtained using a fluorescence microscope (Leica).

2.12. Cell cycle progression

BEAS-2B cells were seeded overnight in a 12-well plate at 2.5×10^5 cell/ml and exposed to 50 μg/ml pristine or treated SWCNTs for 24 h. Subsequently, the cells were collected, washed with PBS, centrifuged at 1500 rpm for 6 min, and fixed overnight in 2 ml of 70% ethanol (Sigma) and at −20 °C. Upon ethanol fixation, the cells were again washed with PBS, resuspended in 0.2% Tween-20 for 15 min, treated with 10 μl 0.05% RNase for 15 min and stained with 30 μl PI. The DNA content was determined using BD LSR Fortessa Flow

cell analyzer (BD Biosciences) by recording 20,000 events for each sample being analyzed; analyses were performed using the FlowJo software V10.0.7 (Tree Star Inc.).

2.13. Statistical analysis

All results are presented as mean ± standard deviation. Two-way analysis of variance (ANOVA) and unpaired two-tailed Student's *t*-test were performed using JMP 8.0 (SAS Institute) and SigmaPlot 10.0 (Systat Software Inc.). Protein loading and functionality analyses were performed prior to each uptake experiment, with a minimum of 6 independent measurements for each type of sample being investigated. Membrane imaging and migration analyses were repeated 3 times, with at least 10 random fields of view were inspected for each sample in every trial. Western blots were performed in duplicates and repeated 3 times for each protein investigated. All other experiments (uptake, cell cycle, viability) were performed in triplicates and repeated at least 3 times, for a total of minimum 9 replicates per each sample. Results were considered significant when $*p < 0.05$.

3. Results and discussion

3.1. Effects of acids treatment on the physicochemical properties of pristine SWCNTs

SWCNTs with user-tailored properties were prepared from pristine (as manufactured) scaffolds by using multi-step oxidative acids treatment (Dong et al., 2013). Upon 3 and 6 h acids treatment, the resulting SWCNTs denoted as user-tailored SWCNTs were evaluated for any changes in their physicochemical characteristics (Dong et al., 2013; Marshall et al., 2006; Eldawud et al., 2015b). Raman analysis showed that the intensity ratio between the D (treatment-induced disorder) and G (treatment-induced change in purity) peaks (I_D/I_G) were 0.210 ± 0.1 for the 3 h and 0.47 ± 0.05 for the 6 h treated samples. These were correspondingly 16% lower and 85% higher than the I_D/I_G of pristine SWCNTs (Table 1; Supporting Fig. 1). The significant increase in the I_D/I_G observed for the 6 h treated sample was associated with the generation of oxygen (O)-related functional groups (Dong et al., 2013; Wepasnick et al., 2010). The average indvidual length of SWCNTs as evaluated by atomic force microscopy (AFM) was reduced by 22% and 43% for the 3 and 6 h acids treated samples, all relative to the pristine one (Table 1). Further, energy dispersive elemental (EDX) analyses showed a reduction in the metal impurities (i.e., Fe, Co, Cl) normally present in the pristine sample, with such reduction being function of the treatment time (Supporting Fig. 2) (Pumera, 2007). The observed differences in the nanotube length and purity are consistent with previous reports showing that strong acid incubation cuts CNTs at their defect sites, removes impurities and generates shorter samples (Dong et al., 2014a; Eldawud et al., 2015b).

Analyses of the average agglomerate size in cellular media as investigated by dynamic light scattering technique (DLS) revealed 40 and 22% reduction for the 3 and 6 h treated samples respectively, all relative to the pristine SWCNTs (Supporting Fig. 3). The difference in the agglomerates size is presumably a result of the interplay between the van der Waals attraction forces exerted between individual nanotubes and the electrical repulsion forces generated by the O-rich functional groups induced on their surface upon suspension in the serum rich media as described by the Schulze-Hardy rule (Desai et al., 2014; Sano et al.,

2001). Such difference also led to an increase in dispersity by 176% and 200% in deionized water and 70% and 90% in cellular media respectively, for the 3 h and 6 h acid treated samples when compared to the pristine one (Supporting Fig. 4).

3.2. Uptake of user-tailored SWCNTs is function of their physicochemical properties

Such characterized user-tailored nanotubes were further exposed to model cellular systems used for lung inhalation studies (Dong et al., 2013; Dong et al., 2014a; Eldawud et al., 2015a). Briefly, the samples were first fluorescently labeled with 488 Alexa-labeled Bovine Serum Albumin (Alexa-BSA) through physical (for pristine) or covalent chemistry (for the treated samples) (Dong et al., 2013; Eldawud et al., 2015a; Dong et al., 2014b) to form Alexa-BSA-SWCNT conjugates. Secondly, the samples were dispersed in cellular media by sonication, and subsequently exposed to immortalized human lung epithelial cells (BEAS-2B) for 24 h. Alexa-BSA labeling was previously used as a suitable method to allow for tracking nanomaterials uptake in cellular systems (Dong et al., 2014a; Holt et al., 2011). The 50 μg/ml nanotube exposure dose was chosen based the recommendation made by the Occupational Safety and Health Administration (OSHA) for particles less than 5 μm in diameter. The dose reflects acute worker exposures for 14 years at 40 working hour a week and is similar both to the levels of SWCNTs currently recorded in working areas (ranging between 0.7 and 53 $\mu g/m^3$) as well as to estimates of SWCNTs on individual worker gloves (ranging between 217 μg to 6020 μg) (Maynard et al., 2004b; Jeong Hee et al., 2008b).

Spectroscopical analyses based on estimating the relative amount of Alexa-BSA immobilized onto SWCNTs known as the loaded protein and excluding the individual signals of the protein or nanotubes alone, showed that loading was function of the physicochemical properties of the sample being used, with physical interactions of the protein to the pristine SWCNTs leading to 0.28 ± 0.04 mg protein loaded per mg of the nanotube. Complementarily, covalent interactions through zero length chemistry led to 0.30 ± 0.05 and 0.36 ± 0.02 mg protein per mg of 3 and 6 h treated SWCNTs respectively, with the loading onto the 6 h treated sample being significantly higher than both the loading onto the pristine and 3 h sample respectively.

The differences in protein loading were presumably associated with the different surface properties of both the Alexa-BSA and the nanotube being used (e.g., surface chemistry, charge and surface area), and differences in the mechanisms of protein binding, i.e., physical versus covalent respectively (Campbell et al., 2014). Specifically, previous analyses have showed that physical binding of proteins onto nanotubes leads to unstable multi-point attachment geometries and protein deformation. Such changes are also known to be dependent on the available nanotube and protein surface area, agglomerate size, and the individual protein-nanotube interactions respectively (Campbell et al., 2014). Complementarily, covalent binding was shown to reduce protein deformation and led to more stable interactions of the immobilized protein and the nanotube most likely due to the integration of O-related functional groups as anchors in the zero-length single point attachment (Dong et al., 2013; Campbell et al., 2014; Campbell et al., 2013). The lower protein loading values observed for pristine SWCNTs could also be associated with the limited available surface area for protein binding, since DLS analyses showed that larger

agglomerates were observed for such nanotubes. Similarly, the higher loading recorded on the 6 h treated SWCNTs when compared to the 3 h treated sample could be presumably associated with the higher number of O-related functional groups that such nanotubes would have (as confirmed by Raman and EDX analyses) to be used as functional zero-chemistry anchors.

The functionality of the immobilized fluorophore was assessed to eliminate concerns associated with reduced ability to evaluate nanomaterial uptake in the BEAS-2B cellular system. For this, spectroscopical analyses of the height of the absorbance peaks of the immobilized and free protein respectively (Dong et al., 2014b) were performed, with results showing that the physically immobilized Alexa-BSA retained about 32 ± 4%, while covalently immobilized protein retained 39 ± 5% and 71 ± 4% functionality at the 3 and 6 h treated SWCNT interfaces respectively, all relative to the free Alexa-BSA in solution or non-labeled SWCNTs (Fig. 1a,b,c). The higher functionality observed for the Alexa-BSA immobilized onto the 6 h treated SWCNTs relative to both 3 h treated and pristine nanotube samples is presumably associated with the more hydrophilic nature of the first listed nanotubes. Specifically, the overall protein and nanomaterial electric properties, as well as the changes in the surrounding environment caused by the higher degree of hydration of the sample as a result of their higher O-groups was previously shown to induce reduced protein deformability and thus be responsible for less quenching at nanotube interface (Brege et al., 2009; Chiu et al., 2011).

Cellular ability to take up fluorescently labeled user-tailored SWCNTs or pristine counterparts was subsequently evaluated using Fluorescence Activated Cell Sorting (FACS; Fig. 1d) and reported relative to controls (i.e., unexposed cells, cells exposed to unlabeled SWCNTs, and cells exposed to free Alexa-BSA in amounts equivalent to the amount of protein loaded onto the individual nanotubes). Results showed that while there were no significant differences between controls of unexposed cells and cells exposed to pristine, 3 or 6 h treated SWCNTs respectively, the fluorescent signal of the cells exposed to Alexa-BSA-SWCNT conjugates was significantly higher than that of the controls. Furthermore, about 23% and 37% significantly higher intensity was recorded for the cells exposed to the 6 h treated SWCNTs relative to cells exposed to the 3 h or pristine SWCNT samples respectively.

The observed differences are presumably associated with either (Mauter and Elimelech, 2008) higher cellular uptake as induced by the presence of a higher number of 6 h treated nanotubes relative to the other samples (smaller sizes), and/or (Jorio and Dresselhaus, 2003) the different loading and functionality of the bound fluorophore onto the user-tailored or pristine SWCNTs. With regards to the former, previous studies have shown that a size-driven SWCNTs uptake occurs either via endocytosis and/or diffusion (Antonelli et al., 2010), with results indicating that shorter and more hydrophilic SWCNTs are preferentially taken up at faster rates relative to their longer and more hydrophobic counterparts (Prato et al., 2008; Kam et al., 2006). For the latter, the different surface properties of both the protein and individual nanotubes (i.e., surface chemistry, charge and surface area etc.) is known to influence the mechanisms of protein binding (Campbell et al., 2014), with the reduction in the fluorophore functionality being related to either the quenching or the protein

deformability at the nanotube interface. Previous studies have also showed that the energy and electron transfer at the SWCNT surface could hydrolyze and deactivate the excited fluorophores (Yang et al., 2008), while immobilization of the proteins onto nanotubes could lead to protein deformation and subsequently reduced functionality (Campbell et al., 2014; Campbell et al., 2013; Dinu et al., 2010).

3.3. Exposure to user-tailored SWCNTs influences the overall cellular fate

Since previous analyses revealed that internalized SWCNTs reduce cellular viability, and knowing that apoptosis and necrosis are major forms of programmed/triggered cell death (Kroemer et al., 2009), we evaluated cellular distributions according to their viability statuses (Fig. 2). Specifically, our analyses of the percentages of viable, apoptotic and necrotic cells showed that the short-term exposure used in this study (24 h) to 50 μg/ml sample has significantly induced higher percentage of cells at the late apoptotic and necrotic stages relative to control (unexposed) cells. Specifically, exposure to pristine, 3 and 6 h treated SWCNTs showed significantly higher percentages of cells in late apoptosis (i.e., 10%, 5% and 4.5% respectively) all compared to control cells (2%). Significantly higher percentages were observed for cells exposed to pristine SWCNTs when compared to cells exposed to the treated SWCNTs. Lastly, the percentage of necrotic cells was significantly higher, with exposures to pristine leading to 4.3%, and exposure to 3 and 6 h treated SWCNTs leading to 3.45% and 2.9% changes respectively, all relative to control cells. These analyses are supported by previous studies that showed that SWCNTs with a higher percentage of metal impurities (i.e., Fe > 26 wt%) and larger agglomerate size (~20 μm) reduce cellular viability more so than purified (0.23 wt% of Fe) and short SWCNTs (0.5–2 μm) respectively (Wang et al., 2011; Kagan et al., 2006). While such analyses do not necessarily reflect the biochemical mechanisms associated with cellular loss of functionality(Kroemer et al., 2009) nor determine the relationships between apoptotic/necrotic cell death and the induced cellular toxicity, they suggest different mechanisms for the cellular changes induced by the exposures to different user-tailored nanotubes.

3.4. Exposure to SWCNTs with different physicochemical properties affects cell-cell contacts and cellular monolayer integrity

Previous studies have investigated the effects of SWCNTs on cell morphology with results revealing irregular shapes and membrane ruffles following exposure and nanotube uptake (Tian et al., 2006). However, limited information exists on the effects of SWCNTs exposure on the epithelial layer monolayer integrity and cell-cell connections (Kaiser et al., 2008). Knowing that cellular connections and cellular monolayer integrity play critical roles in maintaining differentiated cellular phenotypes (Braga et al., 1999) and further, knowing that monolayer integrity regulates cellular functions from growth, to spreading, to cytoskeletal organization, cellular migration, proliferation, and viability respectively (Knights et al., 2012; Van Marck and Bracke, 2000–2013; Fernandez-Vidal et al., 2006; Jean and Simmons, 1999), we evaluated SWCNT-induced changes in cellular morphologies.

Our qualitative visual optical microscopy analyses revealed a lower confluence level and thus reduced cell-cell interactions upon exposure to both pristine and user-tailored nanotubes, all relative to control cells (Fig. 3, Panel 1). The apparent changes in confluence

levels suggested that exposure to nanotubes with different physicochemical properties lead to changes in the membrane integrity and/or induced membrane damage (Shimizu et al., 2013). Complementarily, bright field image analyses showed that upon cellular exposure the nanotubes seemed to accumulate or localize around and/or at the nuclear regions (Fig. 3, Panel 2). These results are supported by previous analyses that showed preferential internalization of short, functionalized (acid treated) SWCNTs when compared to their pristine counterparts (Maynard et al., 2004a; Antonelli et al., 2010), with the extent of internalization being tightly regulated by the nature and the intensity of CNT-membrane interactions, as well as by the local perturbation induced at the nanotube-lipid bilayer interfaces (Lelimousin and Sansom, 2013). Furthermore, previous reports have indicated localization of the nanotubes around, inside and at the perinuclear region of the cells and suggested possible association of such localized nanotubes with DNA, cytoskeletal elements, and/or cellular centrosomes to induce deleterious effects on the cellular genetic elements (Sargent et al., 2010; Siegrist et al., 2014; Sargent et al., 2009). Indeed, our analysis of the nuclear changes (Fig. 3, Panel 3) obtained by scoring the percentages of cells with nuclear abnormalities resulted upon exposure, showed a significant increase in nuclear deformation for cells exposed to 3 and 6 h acid treated SWCNTs respectively relative to controls and pristine SWCNTs (Supporting Fig. 5).

3.5. Effects of SWCNT's exposure on cell-cell and cell-substrate regulatory proteins

Taking into account the observed changes in cell-cell contacts and nuclear morphologies we investigated whether such changes also affect the expression of major proteins (namely Rac 1/2/3, vimentin, E-cadherin, and vinculin). The hypothesis is based on previous studies that showed that such changes could influence cellular behavior (Mani et al., 2008), be associated with complex interactions with cytoskeletal elements (Pawlak and Helfman, 2001), and lead to cell transformation and carcinogenesis (Knights et al., 2012; Kalluri and Weinberg, 2009). Specifically, Rac 1/2/3 complex is known as an active protein regulator complex and a hallmark for regulating cytoskeletal and adherent junction dynamics (Asai et al., 2011; Allen et al., 1997), vimentin is a type III intermediate filament protein responsible for maintaining cell shape, integrity, and stabilizing cytoskeletal interactions (Kim et al., 2010; McInroy and Määttä, 2007), E-cadherin is the primary protein responsible for cellular adhesion, cell-cell contacts and EMT (Abe et al., 2008; Li et al., 2007), while vinculin is a cytoskeletal protein that regulates adhesion junctions, focal adhesion points (Márquez et al., 2014), and epithelial biogenesis (Theys et al., 2011; Peng et al., 2010).

Our analysis of Rac 1/2/3 complex showed a 38, 59 and 64% reduction in its expression levels for cells exposed to pristine, 3 and 6 h treated SWCNTs respectively, all relative to control cells (Fig. 4a). Expression was also fully reduced for vimentin, with analysis showing 25, 35, and 45% significant reduction following exposure to pristine, 3 and 6 h treated SWCNTs respectively, again, all relative to control cells. Our results are supported by previous studies that showed that Rac acts as a key molecule to regulate responses by reorganization of vimentin filaments(Lee et al., 2001) and thus inhibiting Rac could lead to inhibition of vimentin regulation mostly resulting from the changes in mechanical homeostasis of the cells (Murray et al., 2014). Expression of E-cadherin and vinculin was

only reduced for cells exposed to user-tailored nanotubes by 30 and 35% for the 3 h treated and 41 and 30% for the 6 h treated samples respectively, all relative to control cells.

Considering that vinculin regulates adherent junctions and that the absence of vinculin leads to impaired epithelial cell-cell/substrate adhesion due to a decrease in cell-surface expression of E-cadherin (Peng et al., 2010), our observation suggests that the loss of vinculin from the adhesion sites upon cellular exposure to 3 and 6 h treated nanotubes may be associated with a more aggressive cellular change in response to such user-tailored nanotubes when compared to their pristine counterparts (Wiebe et al., 2000). This hypothesis is supported by previous analyses that showed that the Rac system is responsible for coordinating the dynamic organization and maintenance of the E-cadherin–based cell–cell adherent junctions (Izumi et al., 2004), with a reduction in the Rac expression being associated with cell transformation while still being cell specific (Aznar et al., 2004). Further, it is also supported by other studies that also showed that suppression of E-cadherin is being regarded as a molecular event responsible for the dysfunction in cell-cell adhesion and thus possibly associated with increased invasiveness observed in SWCNT-induced tumors (Luanpitpong et al., 2014) while considering that reduction in the expression of vinculin is compromising cell migration (Rubashkin et al., 2014).

Indeed, optical images (Fig. 4b) and analysis (Fig. 4c) of ability for cellular migration performed upon cellular exposure to the user-tailored nanotubes showed a significant reduction in the number of migrated cells upon treatment with pristine (65%) and 3 h treated SWCNTs (55%), both relative to control cells. However, exposure to 6 h treated SWCNTs did not reveal any significant changes relative to control cells. These results combined with the lower E-cadherin expression levels observed for these cells suggest that reduction in vimentin expression might be responsible for causing EMT (Yeh et al., 2010), however in a different manner than for the cells exposed to 3 h acid treated or pristine nanotubes (Zong et al., 2014). Such results further support the differentiated cellular behavior based on the physicochemical properties of the samples being studied. In particular, based on the role of vimentin-involved EMT phenotype to be mediated using Slug signaling (Vuoriluoto et al., 2011) and with quantitative results showing that with vimentin depletion Slug protein expression significantly decreases, the reduction in Slug may induce initiation of EMT (Medici et al., 2008) for the cells exposed to 6 h treated nanotubes at an even faster rate than for the one exposed to the 3 h sample. Such a hypothesis is supported by the role of vimentin as a downstream effector of the Slug-mediated EMT process where the control of Slug expression was shown to promote EMT-related cancer malignancy (Medici et al., 2008).

Based on these results and considering that cellular transformation is a collaborative event coordinated by key oncogenic pathways, the observed changes induced by exposure to nanotubes with different physicochemical properties (e.g., size, agglomerate size, surface chemistry) provide evidence for a diversified signaling mechanism and changes in cell fate. Such changes seem to be driven by convergence of multiple signaling molecules that affect cell–cell contact and adhesion. Our hypothesis herein is supported by previous studies that indicated that uptake of short, hydrophilic SWCNTs lead to direct interactions with transmembrane proteins (e.g., integrins), reduced cell adhesion and altered cell morphology (Kaiser et al., 2008; Kaiser et al., 2013). Our findings also complement previous reported

analyses that employed an electric impedance sensing platform for real-time analysis to show a significant reduction in cell-cell contact and cell adhesion following exposure to the acid treated SWCNTs when compared to the pristine samples (Eldawud et al., 2015a). Lastly, our data is supported by previous results that showed that cells exposed to nanotubes manifest changes in their migration capability in vitro, and tumor-initiating capability in vivo (Luanpitpong et al., 2014). With E-cadherin regulating cellular migration (Palacios et al., 2002) and with changes in the assembly/disassembly of adherent junctions contributing to the acquisition of migratory potential (Izumi et al., 2004), and knowing that Rac can mediate the loss of adherent junctions and promote a more invasive phenotype (Sander et al., 1998), our observations support the previous formulated hypothesis that the reduction of E-cadherin levels causes mesenchymal cells to detach from one another and from neighboring epithelial cells. It is expected that such events could be correlated with increased invasiveness and metastasis of tumors (Pećina-Šlaus, 2003) upon exposures to nanotubes (Luanpitpong et al., 2014).

3.6. Effects of SWCNTs exposure on cellular proliferation and DNA damage

Taking into account that the observed changes in the expression of major proteins responsible for the formation and maintenance of cell contacts and morphologies could lead to internal cellular transformation and carcinogenesis (Knights et al., 2012; Kalluri and Weinberg, 2009), and also considering the optical observations showing nanotubes localization at or around cells nuclei, we further investigated cell cycle progression. We hypothesize that if changes are to be detected they could be potentially associated with malignant phenotypic transformation to possibly reflect cell senescence and/or apoptosis (Mallette et al., 2007; Richter et al., 1991; Chen et al., 2012).

Our results showed that exposure to pristine SWCNTs led to a 27% significant increase in the percentage of cells at the G1 (gap) phase and a 29% decrease in the percentage of cells at S (synthesis) phase, all relative to control cells. This presumably indicated an early cell cycle arrest at the G1/S phase (Fig. 5a) and could lead to induction of senescent cells (Burton, 2009; Campisi, 2005). Contrary, cells exposed to user-tailored SWCNTs showed increases of 33 and 25% in their percentage at the G2 phase for 3 and 6 h treated SWCNTs respectively, all relative to cells exposed to pristine SWCNTs. This result potentially implies a cell cycle arrest at the G2/M phase or at the G0 phase (Table 2). The arrest at the G2 phase could potentially indicate a mitotic checkpoint response (Sargent et al., 2012) and/or an aggressive EMT transition (Lovisa et al., 2015).

To test whether the observed changes could be a sign of induction of senescence, we evaluated changes in the expression levels of Cdc 25a. Cdc 25a is known as a dual-specificity phosphatase protein involved in the G1/S transition and tightly associated with DNA damage and senescence (Fernandez-Vidal et al., 2006). Quantification of expression levels (Fig. 5b) showed 20, 31 and 60% significant reduction upon exposure to pristine, 3 and 6 h treated SWCNTs respectively, all relative to control cells. Complimentarily, the expression of Cdc 2 (Fig. 5b), a regulatory protein required for passage through control check point, known to regulate linkages of actin to adherent junctions via Rac1, and considered a marker for cellular senescence (Dalton, 1992; Gotzmann et al., 2004), also

showed 52, 31 and 23% significant reduction following cellular exposure to pristine, 3 and 6 h treated SWCNTs respectively.

The significant reduction in the expression of Cdc 2 and Cdc 25a relative to control ß actin is presumably associated with the SWCNTs' ability to induce DNA damage and reduce the intracellular levels of adhesion and/or structural regulatory proteins. Such observations complement previous extensive studies (Allen et al., 1997; Dalton, 1992; Olson et al., 1995). Moreover, our observations are supported by previous analyses that showed that a reduction in cellular adhesion is associated with a downregulation in Cdc 25a, which could result in a de-accelerated S-phase entry, G1 arrest and senescence (Fernandez-Vidal et al., 2006). Lastly, in early studies, it was demonstrated that Rac protein signaling pathway promotes DNA synthesis in the nucleus and is linked directly to the G1/S phase transition in the cell cycle, with reduction in Rac previously shown to result in cell cycle arrest at G1(Allen et al., 1997; Ridley, 2001) as observed for the cells exposed to the pristine SWCNTs.

Our study provides comprehensive analyses of cellular fate as a function of exposure to user-tailored SWCNTs and show differential uptake and SWCNTs' physicochemical-induced cyto- and genotoxic cellular effects respectively. The observed cellular changes could potentially result in alterations in both cell cycle and cellular arrest at an early stage (i.e., G1/S), as well as changes in cell-cell connections and relevant proteins responsible for maintaining cell fate and ultimately indicate differential ability of user-tailored SWCNT to induce cellular transformation. We thus could state that dissecting the physicochemical characteristics of SWCNTs and how they contribute to the differential cellular effects associated with nanotube-induced cellular toxicity could provide insights into how to regulate cell–cell adhesions and cell cycle, to possibly control cellular transformation. Thus, looking into the future and the challenging objective of integrating SWCNTs into biomedical applications, nanotube structure-cellular function relationships need to be established so that cellular transformation is anticipated when versatile and multifunctional user-manipulation of SWCNTs' physicochemical properties is implemented.

4. Conclusions

Through our systematic analyses we conclude that active hallmarks related to cell transformation are being controlled by exposure to usertailored SWCNTs. Specifically, we have shown that higher length, higher metal content and larger agglomerate size of pristine SWCNTs could provide a larger surface area for association and interaction of such nanotubes with various cellular proteins and cellular structures, to possibly reduce cell viability all relative to the changes induced by exposure to 3 and 6 h treated samples which have different physicochemical properties than their counterparts. Further, our analyses show differential uptake and nanotubes-induced cyto- and genotoxic effects, with the induced cellular and DNA-based changes being presumably driven by a variety of factors including metal impurities, length, agglomerate size, surface area, dispersion, and/or SWCNT surface functionalization. In particular, the higher length, higher metal content and larger agglomerate size of pristine SWCNTs could provide a larger surface area for association and interaction with various cellular proteins and organelles to possibly induce higher levels of cellular stress and reduced cell viability relative to the changes induced by the 3 and 6 h acid

treated samples. Such changes could further lead to structural damages that affect cellular migration capabilities and result in alterations of cell cycle and cellular arrest at an early stage (i.e., G1/S), as well as changes in cell-cell connections and relevant proteins responsible for maintaining cell fate.

Supplementary Material

Refer to Web version on PubMed Central for supplementary material.

Acknowledgements

Support for this research was provided through the National Science Foundation (NSF 1434503) and the National Institute of Health (NIH; R01-ES022968). Flow cytometry experiments were performed in the Flow Cytometry Core Facility at WVU; the Core Facility is in part supported by the National Institute of Health equipment grant number S10OD016165 and the Institutional Development Award (IDeA) from the National Institute of General Medical Sciences, P30GM103488 (CoBRE), of the National Institutes of Health under grant number P20GM103434 (INBRE).

References

Abe M, Sugiura T, Takahashi M, Ishii K, Shimoda M, Shirasuna K, 2008 A novel function of CD82/KAI-1 on E-cadherin-mediated homophilic cellular adhesion of cancer cells. Cancer Lett. 266 (2), 163–170. [PubMed: 18395972]

Adhikary A, Chakraborty S, Mazumdar M, Ghosh S, Mukherjee S, Manna A, Mohanty S, Nakka KK, Joshi S, De A, Chattopadhyay S, Sa G, Das T, 2014 Inhibition of epithelial to mesenchymal transition by E-cadherin up-regulation via repression of slug transcription and inhibition of E-cadherin degradation: dual role of SMAR1 in breast cancer cells. J. Biol. Chem 10.1074/jbc.M113.527267.

Allen WE, Jones GE, Pollard JW, Ridley AJ, 1997 Rho, Rac and Cdc42 regulate actin organization and cell adhesion in macrophages. J. Cell Sci 110 (Pt 6), 707–720. [PubMed: 9099945]

Antonelli A, Serafini S, Menotta M, Sfara C, Pierigé F, Giorgi L, Ambrosi G, Rossi L, Magnani M, 2010 Improved cellular uptake of functionalized single-walled carbon nanotubes. Nanotechn. 21 (42), 425101.

Asai A, Okajima F, Nakajima Y, Nagao M, Nakagawa K, Miyazawa T, Oikawa S, 2011 Involvement of Rac GTPase activation in phosphatidylcholine hydroperoxide-induced THP-1 cell adhesion to ICAM-1. Biochem. Biophys. Res. Commun 406 (2), 273–277. [PubMed: 21316345]

Atieh MA, Bakather OY, Al-Tawbini B, Bukhari AA, Abuilaiwi FA, Fettouhi MB, 2010 Effect of carboxylic functional group functionalized on carbon nanotubes surface on the removal of lead from water. Bioinorg. Chem. Appl 603978 10.1155/2010/603978 [PubMed: 21350599]

Aznar S, Fernández-Valerón P, Espina C, Lacal JC, 2004 Rho GTPases: potential candidates for anticancer therapy. Cancer Lett. 206 (2), 181–191. [PubMed: 15013523]

Benincasa M, Pacor S, Wu W, Prato M, Bianco A, Gennaro R, 2011 Antifungal activity of amphotericin B conjugated to carbon nanotubes. ACS Nano 5 (1), 199–208. [PubMed: 21141979]

Braga VMM, Del Maschio A, Machesky L, Dejana E, 1999 Regulation of cadherin function by Rho and Rac: modulation by junction maturation and cellular context. Mol. Biol. Cell 10 (1), 9–22. [PubMed: 9880323]

Brege JJ, Gallaway C, Barron AR, 2009 Fluorescence quenching of single-walled carbon nanotubes with transition-metal ions. J. Phys. Chem. C 113 (11), 4270–4276.

Burton DGA, 2009 Cellular senescence, ageing and disease. Age 31 (1), 1–9. [PubMed: 19234764]

Campbell AS, Dong C, Dordick JS, Dinu CZ, 2013 BioNano engineered hybrids for hypochlorous acid generation. Process Biochem. 48 (9), 1355–1360.

Campbell AS, Dong C, Meng F, Hardinger J, Perhinschi G, Wu N, Dinu CZ, 2014 Enzyme catalytic efficiency: a function of bio–Nano Interface reactions. ACS Appl. Mater. Interfaces 6 (8), 5393–5403. [PubMed: 24666280]

Campisi J, 2005 Senescent cells, tumor suppression, and organismal aging: good citizens, bad neighbors. Cell 120 (4), 513–522. [PubMed: 15734683]

Chen Y, Qu K, Zhao C, Wu L, Ren J, Wang J, Qu X, 2012 Insights into the biomedical effects of carboxylated single-wall carbon nanotubes on telomerase and telomeres. Nat. Commun 3, 1074. [PubMed: 23011128]

Chiu CF, Dementev N, Borguet E, 2011 Fluorescence quenching of dyes covalently attached to single-walled carbon nanotubes. J. Phys. Chem. A 115 (34), 9579–9584. [PubMed: 21766814]

Dalton S, 1992 Cell cycle regulation of the human cdc2 gene. EMBO J. 11 (5), 1797–1804. [PubMed: 1582409]

Desai C, Chen K, Mitra S, 2014 Aggregation behavior of nanodiamonds and their functionalized analogs in an aqueous environment. Environ. Sci.: Processes Impacts 16 (3), 518–523.

Dinu C, Zhu G, Bale S, Anand G, Reeder P, Sanford K, Whited G, Kane R, Dordick J, 2010 Enzyme-based nanoscale composites for use as active decontamination surfaces. Adv. Funct. Mater 20, 392–398.

Dong C, Campell AS, Eldawud R, Perhinschi G, Rojanasakul Y, Dinu CZ, 2013 Effects of acid treatment on structure, properties and biocompatibility of carbon nanotubes. Appl. Surf. Sci 264 (0), 261–268.

Dong C, Eldawud R, Sargent L, Kashon ML, Lowry D, Rojanasakul Y, Dinu CZ, 2014a Towards elucidating the effects of purified MWCNTs on human lung epithelial cells. Environ. Sci. Nano 10.1039/c4en00102h.

Dong C, Eldawud R, Sargent LM, Kashon ML, Lowry D, Rojanasakul Y, Dinu CZ, 2014b Towards elucidating the effects of purified MWCNTs on human lung epithelial cells. Environ. Sci. Nano 1 (6), 95–603. [PubMed: 25485116]

Dong C, Eldawud R, Sargent L, Kashon M, Lowry D, Rojanasakul Y, Dinu CZ, 2015 Carbon nanotube uptake changes the biomechanical properties of human lung epithelial cells in a time-dependent manner. J. Mater. Chem. B 10.1039/c5tb00179j.

Eldawud R, Stueckle TA, Manivannan S, Elbaz H, Chen M, Rojanasakul Y, Dinu CZ, 2014 Real-time analysis of the effects of toxic, therapeutic and sub-therapeutic concentrations of digitoxin on lung cancer cells. Biosens. Bioelectron 59, 192–199. [PubMed: 24727605]

Eldawud R, Wagner A, Dong C, Rojansakul Y, Zoica Dinu C, 2015a Electronic platform for real-time multi-parametric analysis of cellular behavior post-exposure to single-walled carbon nanotubes. Biosens. Bioelectron 71, 269–277. [PubMed: 25913448]

Eldawud R, Wagner A, Dong C, Rojansakul Y, Zoica Dinu C, 2015b Electronic platform for real-time multi-parametric analysis of cellular behavior post exposure to single-walled carbon nanotubes. Biosens. Bioelectron 10.1016/j.bios.2015.04.044.

Fernandez-Vidal A, Ysebaert L, Didier C, Betous R, De Toni F, Prade-Houdellier N, Demur C, Contour-Galcéra M-O, Prévost GP, Ducommun B, Payrastre B, Racaud- Sultan C, Manenti S, 2006 Cell adhesion regulates CDC25A expression and proliferation in acute myeloid leukemia. Cancer Res. 66 (14), 7128–7135. [PubMed: 16854822]

Georgakilas V, Bourlinos A, Gournis D, Tsoufis T, Trapalis C, Mateo-Alonso A, Prato M, 2008 Multipurpose organically modified carbon nanotubes: from functionalization to nanotube composites. J. Am. Chem. Soc 130 (27), 8733–8740. [PubMed: 18597430]

Gotzmann J, Mikula M, Eger A, Schulte-Hermann R, Foisner R, Beug H, Mikulits W, 2004 Molecular aspects of epithelial cell plasticity: implications for local tumor invasion and metastasis. Mutat. Res. Rev. Mutat. Res 566 (1), 9–20.

Guo W, Dou Z, Li H, Shi Z, Sun H, Liu Y, 2010 An efficient strategy for the purification of cloth-like single walled carbon nanotube soot produced by arc discharge. Carbon 48 (13), 3769–3777.

Herzog E, Byrne HJ, Casey A, Davoren M, Lenz A-G, Maier KL, Duschl A, Oostingh GJ, 2009 SWCNT suppress inflammatory mediator responses in human lung epithelium in vitro. Toxicol. Appl. Pharmacol 234 (3), 378–390. [PubMed: 19041333]

Hitoshi K, Katoh M, Suzuki T, Ando Y, Nadai M, 2011 Differential effects of single-walled carbon nanotubes on cell viability of human lung and pharynx carcinoma cell lines. J. Toxicol. Sci 36 (3), 379–387. [PubMed: 21628966]

Holt BD, Dahl KN, Islam MF, 2011 Quantification of uptake and localization of bovine serum albumin-stabilized single-wall carbon nanotubes in different human cell types. Small 7 (16), 2348–2355. [PubMed: 21626688]

Izumi G, Sakisaka T, Baba T, Tanaka S, Morimoto K, Takai Y, 2004 Endocytosis of E- cadherin regulated by Rac and Cdc42 small G proteins through IQGAP1 and actin filaments. J. Cell Biol 166 (2), 237–248. [PubMed: 15263019]

Jean P, Simmons PJ, 1999 Cytoskeleton and integrin-mediated adhesion signaling in human CD34+ hemopoietic progenitor cells. Exp. Hematol 27 (4), 579–586. [PubMed: 10210315]

Jeong Hee H, Eun Jung L, Ji Hyun L, Kang Pyo S, Young Hee L, Gwi Nam B, Seung-Bok L, Jun Ho J, Myung Haing C, Il Je Y, 2008a Monitoring multiwalled carbon nanotube exposure in carbon nanotube research facility. Inhal. Toxicol 20 (8), 741–749. [PubMed: 18569096]

Jeong Hee H, Eun Jung L, Ji Hyun L, Kang Pyo S, Young Hee L, Gwi Nam B, Seung-Bok L, Jun Ho J, Myung Haing C, Il Je Y, 2008b Monitoring multiwalled carbon nanotube exposure in carbon nanotube research facility. Inhal. Toxicol 20 (8), 741–749. [PubMed: 18569096]

Jorio A, Dresselhaus G, 2003 Fullerenes and Carbon Nanotubes In: Meyers RA (Ed.), Encyclopedia of Physical Science and Technology, Third Edition. Academic Press, New York, pp. 315–335.

Kagan VE, Tyurina YY, Tyurin VA, Konduru NV, Potapovich AI, Osipov AN, Kisin ER, Schwegler-Berry D, Mercer R, Castranova V, Shvedova AA, 2006 Direct and indirect effects of single walled carbon nanotubes on RAW 264.7 macrophages: Role of iron. Toxicol. Lett 165 (1), 88–100. [PubMed: 16527436]

Kah M, Zhang X, Hofmann T, 2014 Sorption behavior of carbon nanotubes: changes induced by functionalization, sonication and natural organic matter. Sci. Total Environ 497–498 (0), 133–138.

Kaiser JP, Wick P, Manser P, Spohn P, Bruinink A, 2008 Single walled carbon nanotubes (SWCNT) affect cell physiology and cell architecture. J. Mater. Sci. Mater. Med 19 (4), 1523–1527. [PubMed: 17990080]

Kaiser JP, Buerki-Thurnherr T, Wick P, 2013 Influence of single walled carbon nanotubes at subtoxical concentrations on cell adhesion and other cell parameters of human epithelial cells. J. King Saud Univ. - Science 25 (1), 15–27.

Kalluri R, Weinberg RA, 2009 The basics of epithelial-mesenchymal transition. J. Clin. Invest 119 (6), 1420–1428. [PubMed: 19487818]

Kam NWS, Liu Z, Dai H, 2006 Carbon nanotubes as intracellular transporters for proteins and DNA: an investigation of the uptake mechanism and pathway. Angew. Chem 118 (4), 591–595.

Karimi M, Solati N, Ghasemi A, Estiar MA, Hashemkhani M, Kiani P, Mohamed E, Saeidi A, Taheri M, Avci P, Aref AR, Amiri M, Baniasadi F, Hamblin MR, 2015 Carbon nanotubes part II: a remarkable carrier for drug and gene delivery. Expert Opin. Drug Deliv 12 (7), 1089–1105. [PubMed: 25613837]

Kim H, Nakamura F, Lee W, Hong C, Pérez-Sala D, McCulloch CA, 2010 Regulation of cell adhesion to collagen via β1 integrins is dependent on interactions of filamin A with vimentin and protein kinase C epsilon. Exp. Cell Res 316 (11), 1829–1844. [PubMed: 20171211]

Knights AJ, Funnell APW, Crossley M, Pearson RCM, 2012 Holding tight: cell junctions and cancer spread. Trends Cancer Res. 8, 61–69. [PubMed: 23450077]

Kroemer G, Galluzzi L, Vandenabeele P, Abrams J, Alnemri ES, Baehrecke EH, Blagosklonny MV, El-Deiry WS, Golstein P, Green DR, Hengartner M, Knight RA, Kumar S, Lipton SA, Malorni W, Nuñez G, Peter ME, Tschopp J, Yuan J, Piacentini M, Zhivotovsky B, Melino G, 2009 Classification of cell death: recommendations of the nomenclature committee on cell death 2009. Cell Death Differ. 16 (1), 3–11. [PubMed: 18846107]

Lee S, Song E, Kim H, Kang H, Kim J, Lee K, 2001 Rac1 regulates heat shock responses by reorganization of vimentin filaments: identification using MALDI-TOF MS. Cell Death Differ. 8 (11), 1093–1102. [PubMed: 11687887]

Lelimousin M, Sansom MS, 2013 Membrane perturbation by carbon nanotube insertion: pathways to internalization. Small 9 (21), 3639–3646. [PubMed: 23418066]

Li L. x., Li F, 2011 The effect of carbonyl, carboxyl and hydroxyl groups on the capacitance of carbon nanotubes. New Carbon Mater. 26 (3), 224–228.

Li Z, Wang L, Zhang W, Fu Y, Zhao H, Hu Y, Prins BP, Zha X, 2007 Restoring E-cadherin-mediated cell–cell adhesion increases PTEN protein level and stability in human breast carcinoma cells. Biochem. Biophys. Res. Commun 363 (1), 165–170. [PubMed: 17845801]

Liu Z, Sun X, Nakayama-Ratchford N, Dai H, 2007 Supramolecular chemistry on water- soluble carbon nanotubes for drug loading and delivery. ACS Nano 1 (1), 50–56. [PubMed: 19203129]

Lovisa S, LeBleu VS, Tampe B, Sugimoto H, Vadnagara K, Carstens JL, Wu C-C, Hagos Y, Burckhardt BC, Pentcheva-Hoang T, Nischal H, Allison JP, Zeisberg M, Kalluri R, 2015 Epithelial-to-mesenchymal transition induces cell cycle arrest and parenchymal damage in renal fibrosis. Nat. Med 21 (9), 998–1009. [PubMed: 26236991]

Luanpitpong S, Wang L, Castranova V, Rojanasakul Y, 2014 Induction of stem-like cells with malignant properties by chronic exposure of human lung epithelial cells to single-walled carbon nanotubes. Part. Fibre Toxicol 11, 22. [PubMed: 24885671]

Mallette FA, Gaumont-Leclerc M-F, Ferbeyre G, 2007 The DNA damage signaling pathway is a critical mediator of oncogene-induced senescence. Genes Dev. 21 (1), 43–48. [PubMed: 17210786]

Mani SA, Guo W, Liao M-J, Eaton EN, Ayyanan A, Zhou AY, Brooks M, Reinhard F, Zhang CC, Shipitsin M, 2008 The epithelial-mesenchymal transition generates cells with properties of stem cells. Cell 133 (4), 704–715. [PubMed: 18485877]

Manke A, Luanpitpong S, Dong C, Wang L, He X, Battelli L, Derk R, Stueckle T, Porter D, Sager T, Gou H, Dinu C, Wu N, Mercer R, Rojanasakul Y, 2014 Effect of fiber length on carbon nanotube-induced Fibrogenesis. Int. J. Mol. Sci 15 (5), 7444–7461. [PubMed: 24786100]

Márquez MG, Brandán YR, Guaytima EV, Paván CH, Favale NO, Sterin-Speziale NB, 2014 Physiologically induced restructuring of focal adhesions causes mobilization of vinculin by a vesicular endocytic recycling pathway. BBA-Mol. Cell. Res 1843 (12), 2991–3003.

Marshall MW, Popa-Nita S, Shapter JG, 2006 Measurement of functionalised carbon nanotube carboxylic acid groups using a simple chemical process. Carbon 44 (7), 1137–1141.

Mauter MS, Elimelech M, 2008 Environmental applications of carbon-based nanomaterials. Environ. Sci. Technol 42 (16), 5843–5859. [PubMed: 18767635]

Maynard AD, Baron PA, Foley M, Shvedova AA, Kisin ER, Castranova V, 2004a Exposure to carbon nanotube material: aerosol release during the handling of unrefined single-walled carbon nanotube material. J. Toxicol. Environ. Health A 67 (1), 87–107. [PubMed: 14668113]

Maynard AD, Baron PA, Foley M, Shvedova AA, Kisin ER, Castranova V, 2004b Exposure to carbon nanotube material: aerosol release during the handling of unrefined single-walled carbon nanotube material. J. Toxic. Environ. Health A 67 (1), 87–107.

McInroy L, Määttä A, 2007 Down-regulation of vimentin expression inhibits carcinoma cell migration and adhesion. Biochem. Biophys. Res. Commun 360 (1), 109–114. [PubMed: 17585878]

Medici D, Hay ED, Olsen BR, 2008 Snail and slug promote epithelial-Mesenchymal transition through β-catenin–T-cell Factor-4-dependent expression of transforming growth factor-β3. Mol. Biol. Cell 19 (11), 4875–4887. [PubMed: 18799618]

Mehdipoor E, Adeli M, Bavadi M, Sasanpour P, Rashidian B, 2011 A possible anticancer drug delivery system based on carbon nanotube-dendrimer hybrid nanomaterials. J. Mater. Chem 21 (39), 15456–15463.

Murray ME, Mendez MG, Janmey PA, 2014 Substrate stiffness regulates solubility of cellular vimentin. Mol. Biol. Cell 25 (1), 87–94. [PubMed: 24173714]

Olson M, Ashworth A, Hall A, 1995 An essential role for Rho, Rac, and Cdc42 GTPases in cell cycle progression through G1. Science 269 (5228), 1270–1272. [PubMed: 7652575]

Palacios F, Schweitzer JK, Boshans RL, D'Souza-Schorey C, 2002 ARF6-GTP recruits Nm23-H1 to facilitate dynamin-mediated endocytosis during adherens junctions disassembly. Nat. Cell Biol 4 (12), 929–936. [PubMed: 12447393]

Pawlak G, Helfman DM, 2001 Cytoskeletal changes in cell transformation and tumorigenesis. Curr. Opin. Genet. Dev 11 (1), 41–47. [PubMed: 11163149]

Pećina-Šlaus N, 2003 Tumor suppressor gene E-cadherin and its role in normal and malignant cells. Cancer Cell Int. 3, 17. [PubMed: 14613514]

Peng X, Cuff LE, Lawton CD, DeMali KA, 2010 Vinculin regulates cell-surface Ecadherin expression by binding to β-catenin. J. Cell Sci 123 (4), 567–577. [PubMed: 20086044]

Plati J, Bucur O, Khosravi-Far R, 2011 Apoptotic cell signaling in cancer progression and therapy. Integr. Biol 3 (4), 279–296 quantitative biosciences from nano to macro.

Podesta JE, Al-Jamal KT, Herrero MA, Tian B, Ali-Boucetta H, Hegde V, Bianco A, Prato M, Kostarelos K, 2009 Antitumor activity and prolonged survival by carbon- nanotube-mediated therapeutic sirna silencing in a human lung xenograft model. Small 5 (10), 1176–1185. [PubMed: 19306454]

Prato M, Kostarelos K, Bianco A, 2008 Functionalized carbon nanotubes in drug design and discovery. Acc. Chem. Res 41 (1), 60–68. [PubMed: 17867649]

Pumera M, 2007 Carbon nanotubes contain residual metal catalyst nanoparticles even after washing with nitric acid at elevated temperature because these metal nanoparticles are sheathed by several graphene sheets. Langmuir 23 (11), 6453–6458. [PubMed: 17455966]

Richter KH, Afshari CA, Annab LA, Burkhart BA, Owen RD, Boyd J, Barrett JC, 1991 Down-regulation of cdc2 in senescent human and hamster cells. Cancer Res. 51 (21), 6010–6013. [PubMed: 1933864]

Ridley AJ, 2001 Rho family proteins: coordinating cell responses. Trends Cell Biol. 11 (12), 471–477. [PubMed: 11719051]

Rubashkin MG, Cassereau L, Bainer R, DuFort CC, Yui Y, Ou G, Paszek MJ, Davidson MW, Chen Y-Y, Weaver VM, 2014 Force engages Vinculin and promotes tumor progression by enhancing PI3K activation of phosphatidylinositol (3,4,5)-triphosphate. Cancer Res. 74 (17), 4597–4611. [PubMed: 25183785]

Sander EE, van Delft S, Jean P, Reid T, van der Kammen RA, Michiels F, Collard JG, 1998 Matrix-dependent Tiam1/Rac signaling in epithelial cells promotes either cell–cell adhesion or cell migration and is regulated by phosphatidylinositol 3-kinase. J. Cell Biol 143 (5), 1385–1398. [PubMed: 9832565]

Sano M, Okamura J, Shinkai S, 2001 Colloidal nature of single-walled carbon nanotubes in electrolyte solution: the Schulze−hardy rule. Langmuir 17 (22), 7172–7173.

Sargent LM, Shvedova AA, Hubbs AF, Salisbury JL, Benkovic SA, Kashon ML, Lowry DT, Murray AR, Kisin ER, Friend S, McKinstry KT, Battelli L, Reynolds SH, 2009 Induction of aneuploidy by single-walled carbon nanotubes. Environ. Mol. Mutagen 50 (8), 708–717. [PubMed: 19774611]

Sargent LM, Reynolds SH, Castranova V, 2010 Potential pulmonary effects of engineered carbon nanotubes: in vitro genotoxic effects. Nanotoxicology 4 (4), 396–408. [PubMed: 20925447]

Sargent LM, Hubbs AF, Young SH, Kashon ML, Dinu CZ, Salisbury JL, Benkovic SA, Lowry DT, Murray AR, Kisin ER, Siegrist KJ, Battelli L, Mastovich J, Sturgeon JL, Bunker KL, Shvedova AA, Reynolds SH, 2012 Single-walled carbon nanotube-induced mitotic disruption. Mutat. Res 745 (0), 28–37. [PubMed: 22178868]

Shimizu K, Uchiyama A, Yamashita M, Hirose A, Nishimura T, Oku N, 2013 Biomembrane damage caused by exposure to multi-walled carbon nanotubes. J. Toxicol. Sci 38 (1), 7–12. [PubMed: 23358135]

Siegrist K, Reynolds S, Kashon M, Lowry D, Dong C, Hubbs A, Young S-H, Salisbury J, Porter D, Benkovic S, McCawley M, Keane M, Mastovich J, Bunker K, Cena L, Sparrow M, Sturgeon J, Dinu C, Sargent L, 2014 Genotoxicity of multi-walled carbon nanotubes at occupationally relevant doses. Part. Fibre Toxicol 11 (1), 6. [PubMed: 24479647]

Smit MA, Peeper DS, 2010 Epithelial-mesenchymal transition and senescence: two cancer-related processes are crossing paths. Aging (Albany NY) 2 (10), 735–741. [PubMed: 20975209]

Smith BR, Ghosn Eliver Eid B, Rallapalli H, Prescher JA, Larson T, Herzenberg LA, Gambhir SS, 2014 Selective uptake of single-walled carbon nanotubes by circulating monocytes for enhanced tumour delivery. Nat. Nanotechnol 9 (6), 481–487. [PubMed: 24727688]

Stepanskiy LG, 2012 Sonication-induced unfolding proteins. J. Theor. Biol 298 (0), 77–81. [PubMed: 22266660]

Theys J, Jutten B, Habets R, Paesmans K, Groot AJ, Lambin P, Wouters BG, Lammering G, Vooijs M, 2011 E-cadherin loss associated with EMT promotes radioresistance in human tumor cells. Radiother. Oncol 99 (3), 392–397. [PubMed: 21680037]

Tian F, Cui D, Schwarz H, Estrada GG, Kobayashi H, 2006 Cytotoxicity of single-wall carbon nanotubes on human fibroblasts. Toxicol. in Vitro 20 (7), 1202–1212 an international journal published in association with BIBRA. [PubMed: 16697548]

Van Marck VL, Bracke ME, 2000–2013 Epithelial-Mesenchymal transitions in human cancer In: Madame Curie Bioscience Database. Landes Bioscience, Austin (TX).

Visalli G, Bertuccio MP, Iannazzo D, Piperno A, Pistone A, Di Pietro A, 2015 Toxicological assessment of multi-walled carbon nanotubes on A549 human lung epithelial cells. Toxicol. in Vitro 29 (2), 352–362. [PubMed: 25499066]

Vuoriluoto K, Haugen H, Kiviluoto S, Mpindi J, Nevo J, Gjerdrum C, Tiron C, Lorens J, Ivaska J, 2011 Vimentin regulates EMT induction by slug and oncogenic H-Ras and migration by governing Axl expression in breast cancer. Oncogene 30 (12), 1436–1448. [PubMed: 21057535]

Wang J, Sun P, Bao Y, Liu J, An L, 2011 Cytotoxicity of single-walled carbon nanotubes on PC12 cells. Toxicol. in Vitro 25 (1), 242–250. [PubMed: 21094249]

Welsher K, Liu Z, Sherlock SP, Robinson JT, Chen Z, Daranciang D, Dai HA, 2009 Route to brightly fluorescent carbon nanotubes for near-infrared imaging in mice. Nat. Nanotechnol 4 (11), 773–780. [PubMed: 19893526]

Wen J, Xu Y, Li H, Lu A, Sun S, 2015 Recent applications of carbon nanomaterials in fluorescence biosensing and bioimaging. Chem. Commun 51 (57), 11346–11358.

Wepasnick KA, Smith BA, Bitter JL, Howard Fairbrother D, 2010 Chemical and structural characterization of carbon nanotube surfaces. Anal. Bioanal. Chem 396 (3), 1003–1014. [PubMed: 20052581]

Wepasnick KA, Smith BA, Schrote KE, Wilson HK, Diegelmann SR, Fairbrother DH, 2011 Surface and structural characterization of multi-walled carbon nanotubes following different oxidative treatments. Carbon 49 (1), 24–36.

Wiebe JP, Muzia D, Hu J, Szwajcer D, Hill SA, Seachrist JL, 2000 The 4pregnene and 5α-pregnane progesterone metabolites formed in nontumorous and tumorous breast tissue have opposite effects on breast cell proliferation and adhesion. Cancer Res. 60 (4), 936–943. [PubMed: 10706108]

Wu H-C, Chang X, Liu L, Zhao F, Zhao Y, 2010 Chemistry of carbon nanotubes in biomedical applications. J. Mater. Chem 20 (6), 1036–1052.

Yang R, Jin J, Chen Y, Shao N, Kang H, Xiao Z, Tang Z, Wu Y, Zhu Z, Tan W, 2008 Carbon nanotube-quenched fluorescent oligonucleotides: probes that fluoresce upon hybridization. J. Am. Chem. Soc 130 (26), 8351–8358. [PubMed: 18528999]

Yeh Y-C, Wei W-C, Wang Y-K, Lin S-C, Sung J-M, Tang M-J, 2010 Transforming growth factor-β1 induces Smad3-dependent β 1 integrin gene expression in epithelial-to-mesenchymal transition during chronic tubulointerstitial fibrosis. Am. J. Pathol 177 (4), 1743–1754. [PubMed: 20709799]

Zehua Q, Guojian W, 2012 Effective chemical oxidation on the structure of multiwalled carbon nanotubes. J. Nanosci. Nanotechnol 12 (1), 105–111. [PubMed: 22523952]

Zong H, Yin B, Zhou H, Cai D, Ma B, Xiang Y, 2014 Inhibition of mTOR pathway attenuates migration and invasion of gallbladder cancer via EMT inhibiation. Mol. Biol. Rep 41 (7), 4507–4512. [PubMed: 24623408]

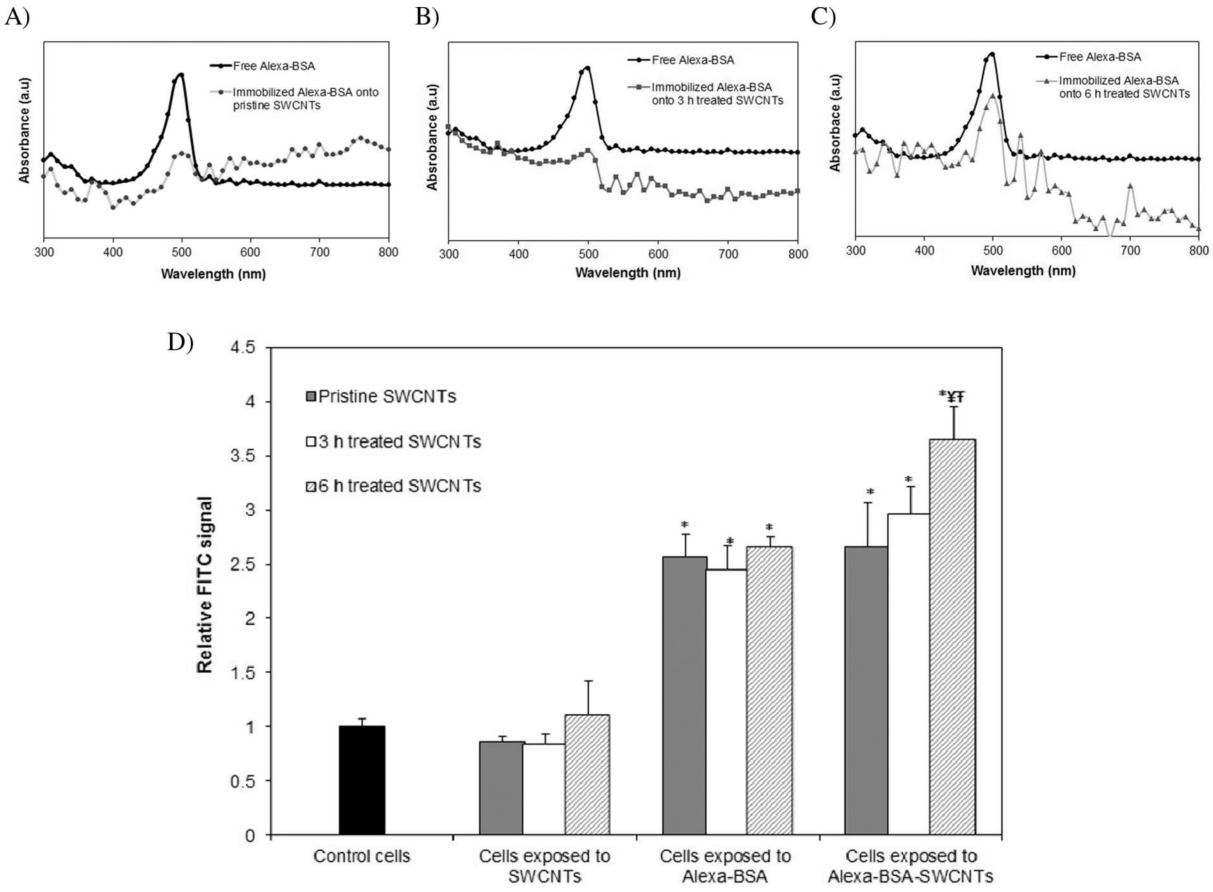

Fig. 1.

Spectroscopical analysis of free and immobilized Alexa-BSA functionality onto: A) pristine, B) 3 and C) 6 h treated SWCNTs. D) Fluorescence Activated Cell Sorting (FACS) analyses confirmed the uptake of fluorescently labeled SWCNTs; results are reported relative to cells exposed to unlabeled SWCNTs, cells exposed to free protein or control cells (unexposed cells) respectively. (*indicates significant difference relative to control cells, ¥ indicates significant difference when compared to cells exposed to pristine SWCNTs, ₸ while indicates signicant differences when compared to cells exposed to 3 h treated SWCNTs respectively, $p < 0.05$).

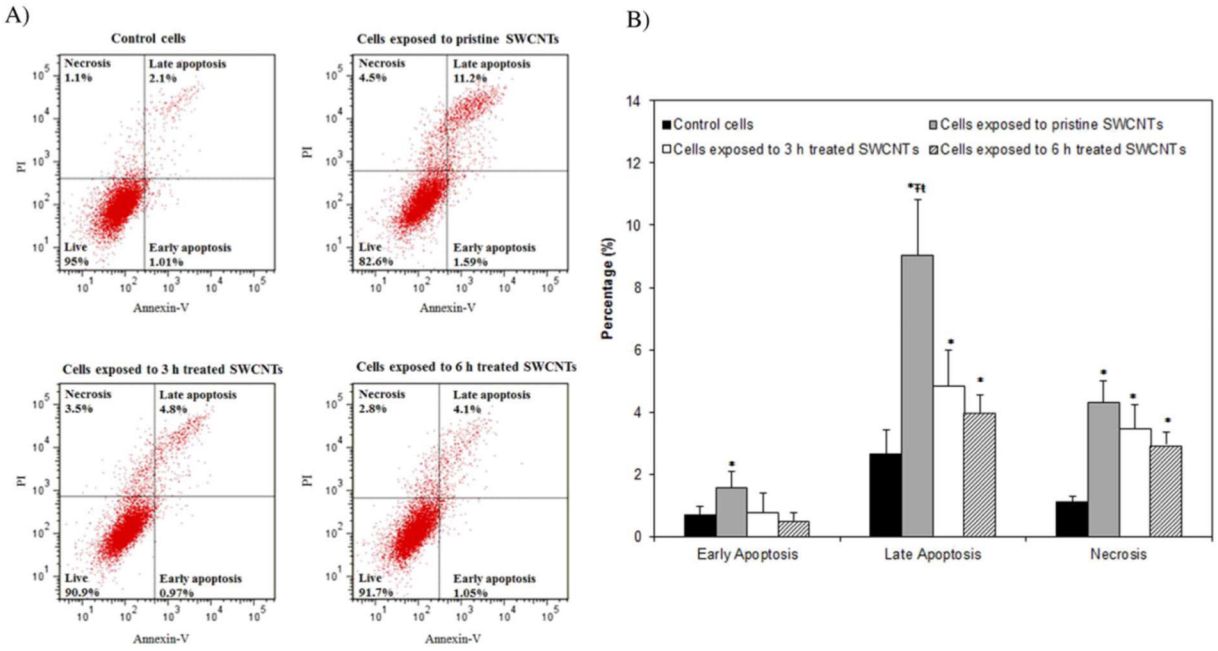

Fig. 2.

Analyses of the cellular viability following exposure to SWCNTs with different physicochemical properties using flow cytometry. A) Histograms of control and SWCNTs exposed cells showing the percentages of cells going through early apoptosis, late apoptosis and necrosis respectively. B) Quantification analyses of cell viability following exposure to SWCNTs with user-tailored properties. (*indicates significant difference relative to control cells, while Ŧ and ǂ indicate significant differences relative to cells exposed to 3 and 6 h treated SWCNTs respectively, all at $p^* < 0.05$).

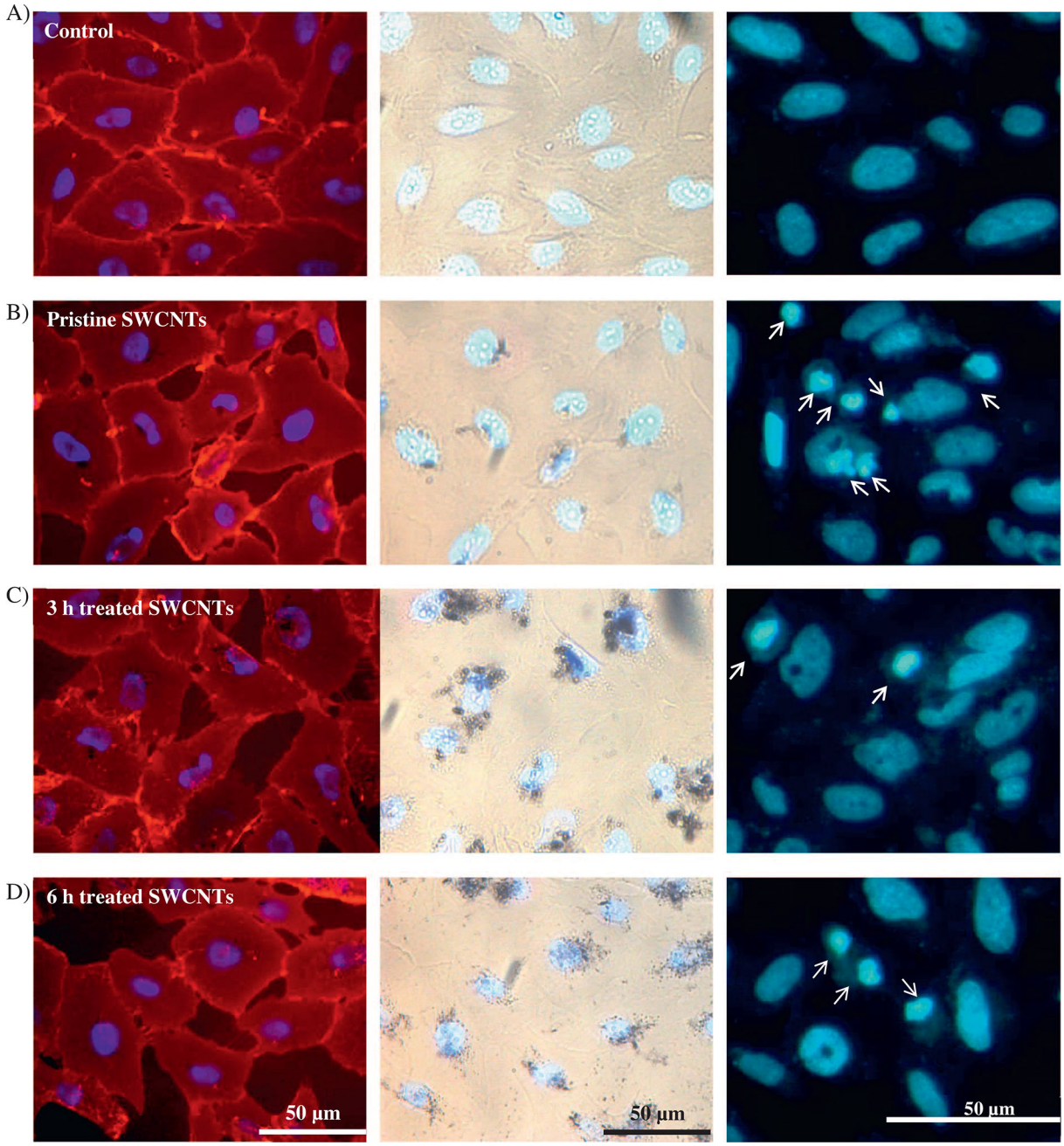

Fig. 3.

Optical microscopy images of BEAS-2B cells exposed to SWCNTs with different physicochemical properties, namely pristine (B), 3 (C) or 6 h (D), all relative to controls (A). Fluorescent images in Panel 1 show changes in the confluence level and their dependency on the SWCNTs physicochemical properties. Panel 2 shows bright field images of the exposed cells, and reveals nanotubes localization at the nucleus or perinuclear region. Panel 3 identified changed nuclear morphologies as resulted upon exposure to user-tailored SWCNTs (arrows).

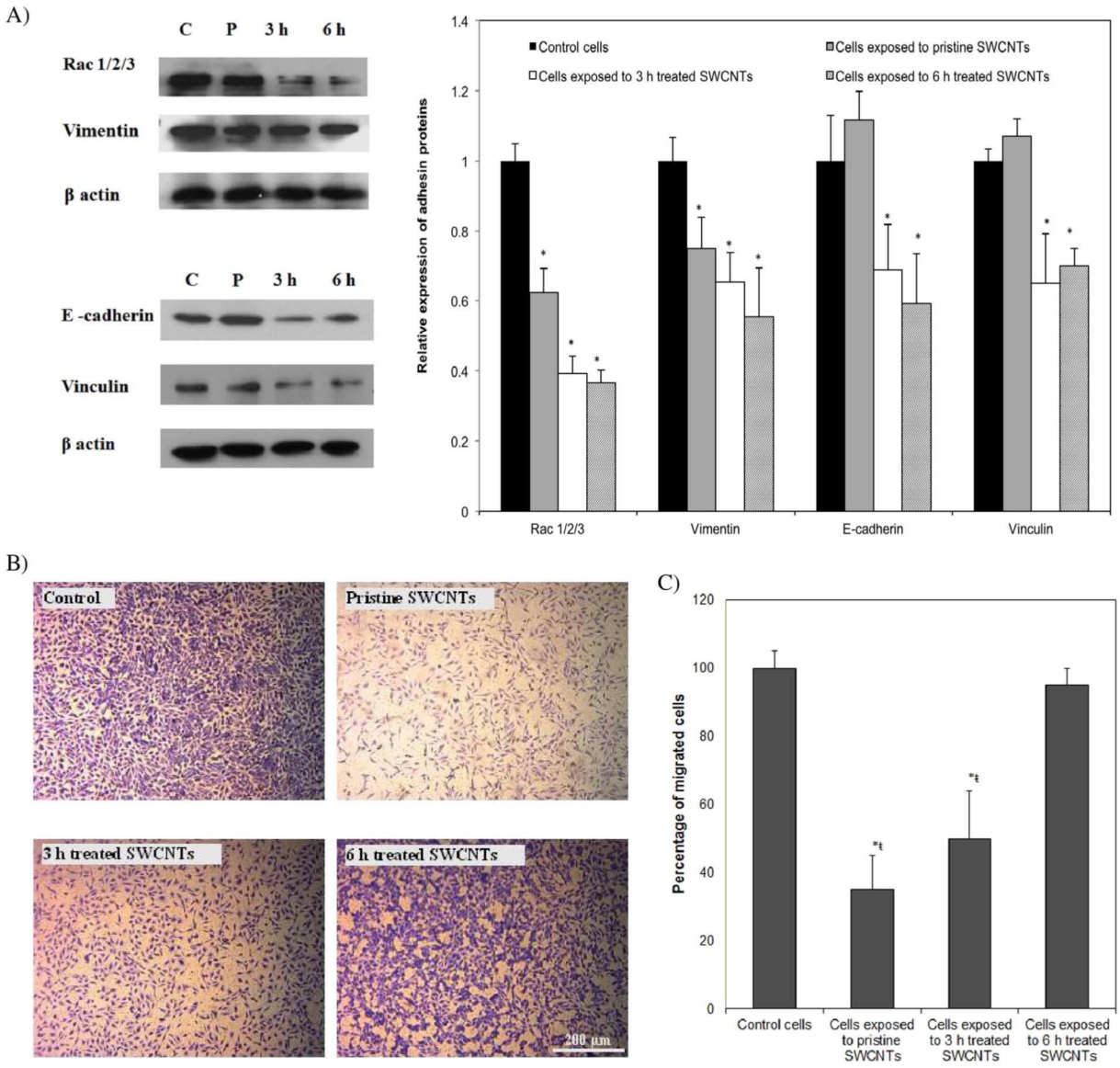

Fig. 4.

A) Western blot analyses and qualification showing differences in the expression of key proteins responsible for cell structure upon cellular exposure to SWCNTs with different physicochemical properties. B) Optical images of migrated cells following 24 h exposure to SWCNTs. C) Qualification of cellular migration ability. (*indicates significant difference relative to control cells, ¥ indicates significant difference when compared to cells exposed to pristine SWCNTs, ₸ and ŧ indicate significant differences when compared to cells exposed to 3 and 6 h treated SWCNTs respectively, $p < 0.05$.

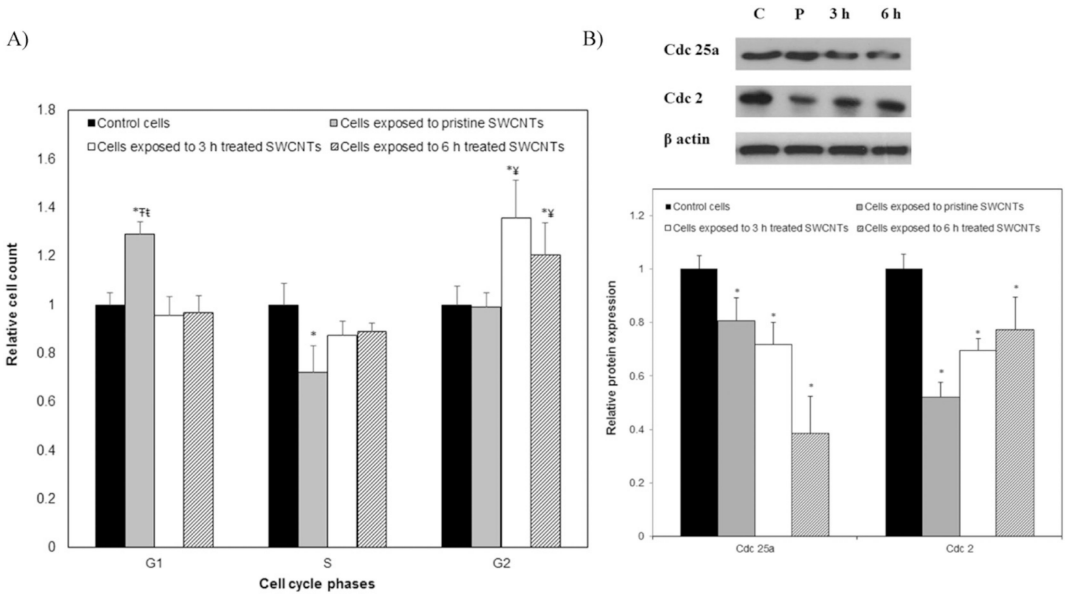

Fig. 5.

A) Percentage of the cells at different cell cycle phases upon 24 h exposure to SWCNTs with different physicochemical properties. B) Western blot analysis of cell cycle regulatory proteins recorded for cells exposed to nanotubes with user-tailored properties. (*indicates significant difference when compared to control cells, ¥ indicates significant difference relative to cells exposed to pristine SWCNTs, Ŧ and ŧ indicate significant differences when compared to cells exposed to 3 h and 6 h acid treated SWCNTs respectively, $p < 0.05$).

Table 1

Analyses of the physical and chemical properties of pristine and user-tailored SWCNTs.

SWCNTs	I_D/I_G	Average length (nm)	Metal percentage (%)	Average agglomerate size (media)	Dispersity in deionized water (mg/ml)	Dispersity in media (mg/ml)
Pristine	0.253 ± 0.05	844 ± 162	10.77	615 ± 133	0.25	0.56
3 h treated	0.210 ± 0.1	656 ± 207	5.49	378 ± 83	0.69	0.96
6 h treated	0.470 ± 0.06	481 ± 95	4.28	481 ± 95	0.75	1.06

Table 2

Cell cycle progression analysis of BEAS-2B cells after exposure for 24 h to pristine and user-tailored SWCNTs.

Sample	G1 (%)	S (%)	G2/M (%)
Control cells	49.70 ± 4.2%	31.50 ± 2.7%	14.80 ± 4.4%
Cells exposed to pristine SWCNTs	63.10 ± 2.7%	22.40 ± 3.5%	14.2 ± 2.4%
Cells exposed to 3 h treated SWCNTs	48.60 + 5.2%	29.10 ± 6.5%	19.80 ± 6.1%
Cells exposed to 6 h treated SWCNTs	48.20 ± 8.1%	28.40 ± 4.8%	18.50 ± 6.3%